Rapid 21st century warming of the Indian Ocean is forced by the Southern Ocean

Abhisek Chatterjee[a,1], Sajidh C K[a], Raghu Murtugudde[b,c], P N Vinayachandran[d] and S S C Shenoi[a]

[a] Indian National Centre for Ocean Information Services, Ministry of Earth Sciences, Hyderabad, India
[b] ESSIC, University of Maryland, College Park, MD, USA
[c] Interdisciplinary Programme in Climate Studies, Indian Institute of Technology, Bombay, India
[d] Centre for Atmospheric and Oceanic Sciences & Divecha Centre for Climate Change, Indian Institute of Science, Bangalore, India

[1] Correspondence: Abhisek Chatterjee; email: abhisek.c@incois.gov.in

Abstract

The tropical Indian Ocean has been warming at an alarming rate in the recent decade with the southern tropical Indian Ocean (STIO; 15°S-35°S) being the hotspot storing more than 40% of the heat absorbed by the Indian Ocean since the 1990s. This also coincides with the "global warming hiatus" marked by an increase of Pacific warm water transport into the Indian Ocean through the Indonesian throughflow (ITF). However, the cause for the basin-wide spread of this warm water has remained unknown. Using observations and reanalysis, we identify the positive phase of the Southern Annular mode and intensification of extratropical westerlies caused by the Southern Ocean warming as the major drivers. We show that westerlies over the Southern Ocean create a strong positive curl and thereby generate westward propagating Rossby waves. Consequently, STIO exhibits a rapid increase in the sea level (4 mm/yr) and a deepening of the thermocline. This leads to an anomalous east-west tilt in the thermocline which drives the spread of warm water into the interior of the basin. Such Southern Ocean forcing of the tropical Indian Ocean assumes a new significance since the Indian Ocean warming is now known to influence the Pacific Ocean response to global warming and accelerate the Atlantic Meridional Overturning Circulation.

Keywords: Climate change, Rossby waves, Anthropogenic Forcing, Pacific Ocean

Introduction

North Indian Ocean (NIO) is semi-enclosed by countries which are home to more than one-third of the global population which are some of the most vulnerable to climate impacts (Roser et al., 2020). The rapid Indian Ocean warming (Nieves et al., 2015; Lee et al., 2015) and associated sea level rise (Thompson et al., 2016; Srinivasu et al., 2017) in the early 21st Century further enhance the vulnerability of this region. The increase of upper ocean temperature also causes damage to the coral reefs endangering the marine biodiversity across the Indian Ocean basin (Zinke et al., 2015). This rapid increase of sea surface temperature of the Indian Ocean has also coincided with the unexpected slowdown of the global SST, also known as the global warming pause or the "hiatus" (Katsman & van Oldenborgh, 2011; Trenberth and Fasullo, 2013; Meehl et al., 2011; Meehl et al., 2014; England et al., 2014). This 21st century hiatus is primarily attributed to a "La-Nina" like negative phase of the Interdecadal Pacific Oscillation (IPO) which enhanced the oceanic heat uptake and strengthened the Pacific trade winds, and brought up cold subsurface waters in the eastern tropical Pacific which soaked up some of the excess heat from anthropogenic forcings. Stronger trade winds also piled-up warm surface water in the western Pacific (Han et al., 2014). Some of these warm waters are advected into the subsurface Southern Tropical Indian Ocean (STIO; Lee et al., 2015; Nieves et al., 2015; Liu et al., 2016; Zhang et al., 2018; Li et al., 2018, 2019) through Indonesian archipelago to increase the upper ocean heat content there (Wijffels et al., 2004; Cai et al., 2005; Feng et al., 2013, 2015). Lee et al. (2015) further added that more than 60% of the extra heat that was absorbed across the global ocean during 2002-2013 is residing in the subsurface waters of the STIO. At decadal timescales, the Indian Ocean shows a basin-wide warming of surface temperature which is frequently

referred to as the Decadal Indian Ocean Basin Mode (IOBM) (Han et al., 2014; Dong and McPhaden, 2017). A positive phase of the IOBM has begun from the beginning of the 21st Century. The mechanism for the persistence of the positive IOBM and its relation to the heat injected from the Pacific into the STIO via the ITF is not fully understood. Hirst and Godfray (1993) suggest that the warm ITF water is partly transported westward by the south equatorial current in the 10°S-15°S latitude band. Rest of the ITF water flows southward via the Leeuwin current down the northwestern and western coasts of the Australia which builds up a coastal sea level gradient culminating in the radiation of Rossby waves from the coast into the interior Indian Ocean (Potemra et al., 2001; Birol and Morrow, 2001). This Rossby wave radiation plays a role in redistributing heat from the west Australian coast into the interior of STIO. Few recent studies, based on the ocean reanalysis products have indicated that the warming in the STIO is primarily driven by the horizontal advection from the ITF region in the recent decades (Zhang et al., 2018; Vidya et al., 2020). However, these studies do not show how this advection takes place within the STIO, primarily because their analyses were mostly based on a box averaged time series in which averaging is done over the entire STIO and therefore, does not resolve the processes that work within the STIO. Note here that owing to the lack of sufficiently long time series of in-situ observations, researchers have mostly relied on limited data available and ocean reanalysis products to understand the underlying processes at multidecadal timescales. However, Jayasankar et al. (2019a, b) argue that not all reanalysis products are reliable for such process studies and note that the reliable one suggests that the

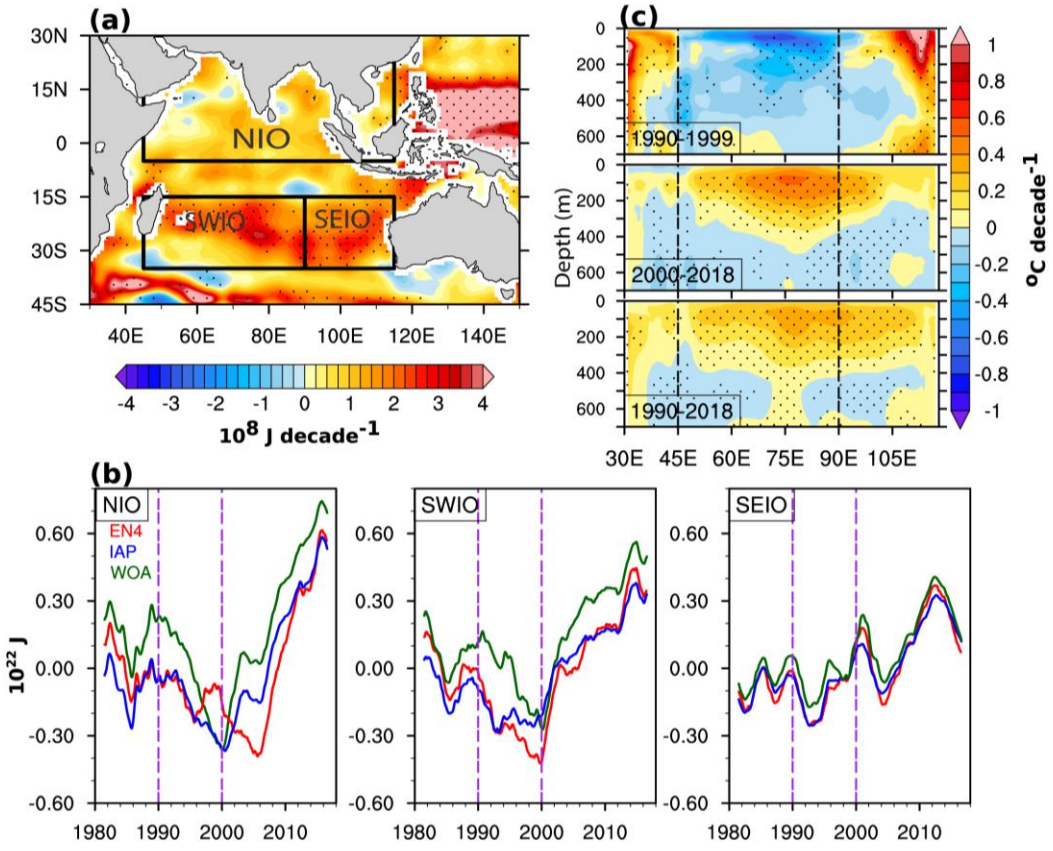

Figure 1. (a) Spatial map of ensemble mean trend of h_{400} from EN4, IAP and WOA for the period 1990-2018 and the black boxes represents SEIO (90°E -115°E and 15°S -35°S), SWIO (45°E -90°E and 15°S -35°S) and NIO (north of 5°N). (b) Time series of h_{400} averaged over NIO, SWIO and SEIO calculated based on EN4, IAP and WOA dataset. (c) Ensemble mean trend of temperature of the upper water column across the STIO averaged over 15°S -35°S during 1990-1999 (upper), 2000-2018 (middle) and 1990-2018 (lower). Stipling in Panels a, c represents regions where the trends calculated based ion EN4 data are 95% significant using two-tailed Student's t-test.

Southern Ocean warming likely contributes to the positive phase of the IOBM.

In other words, the rapid Indian Ocean basin-wide warming is superposed over the enhanced decadal/multidecadal oscillation of the Indian Ocean and studies in the past have mainly linked this to the oceanic and atmospheric changes within and over the Pacific Ocean. The influence of the Southern Ocean on the Indian Ocean warming, however, is still largely unexplored. In this study, we show that the warming in the western part of the STIO and ultimately over the entire IO and its decadal variability is primarily driven by the Southern Annular Mode (SAM; also referred as Antarctic Oscillation or AAO) of the Indian sector of the Southern Ocean and thus link the Indian Ocean warming to the climate change impacts on the Southern Ocean.

Indian Ocean Decadal Variability and the Warming Trend

Upper ocean heat content in the top 400 m water column (h_{400}) derived from objectively analyzed gridded observations (Ensemble mean of EN4, WOA and IAP; see Methods section for more details about these datasets) suggest a basin-wide warming trend during 1990-2018 (Figure 1a and S1). It is observed that the warming of the Indian Ocean is not uniform across the basin. Particularly, the STIO emerges as the warming hotspot of the Indian Ocean storing more than 40% of the total heat absorbed by the Indian Ocean in recent decades. Further, while during 1990-1999 the eastern part of the STIO exhibits rapid coherent warming similar to eastern Pacific, post 2000 that warming hotspot moved westward into the interior of the basin (Figure S1).

Considering the spatial extent of the warming trend (Figure 1a and S1), we have divided the STIO into two regions: (i) South Eastern Indian Ocean (SEIO) extending over 90°E-120°E and 15°S-35°S and (ii) South Western Indian Ocean (SWIO) spanning 45°E-90°E and 15°S-35°S. Additionally, the basin north of 5°N is referred to as the North Indian Ocean (NIO). The analysis of h_{400} time series averaged over SEIO, SWIO and NIO from 1979 to 2018 suggests that these regions do not vary in the same way at decadal/multidecadal timescales (Figure 1b) indicating that mechanisms driving the decadal warming are not uniform across the basin. The SEIO exhibits a prominent decadal variability completing almost three cycles during this period with peaks in the years 1986, 2000 and 2014, respectively, and an increasing trend at a rate of $1.75\pm0.19\times 10^{21}$ J/decade starting from 1993. In contrast, the SWIO shows a prominent decadal variability until 2000 and thereafter a rapid and continuous warming at the rate of $3.71\pm0.17\times10^{21}$ J/decade. Interestingly, NIO also shows a similar variability as the SWIO but with a decadal variability that is much stronger than that over the STIO. The strong decadal variability in the NIO has been noted earlier and attributed to the cross-equatorial heat transport driven by the basin-wide wind-driven circulation that transported warm NIO surface water southward (Thompson et al., 2016; Srinivasu et al., 2017). All three datasets agree with each other for the entire Indian Ocean (Figure S1 and S2) suggesting that the results are robust. The reanalysis product ORAS4 also reproduces the

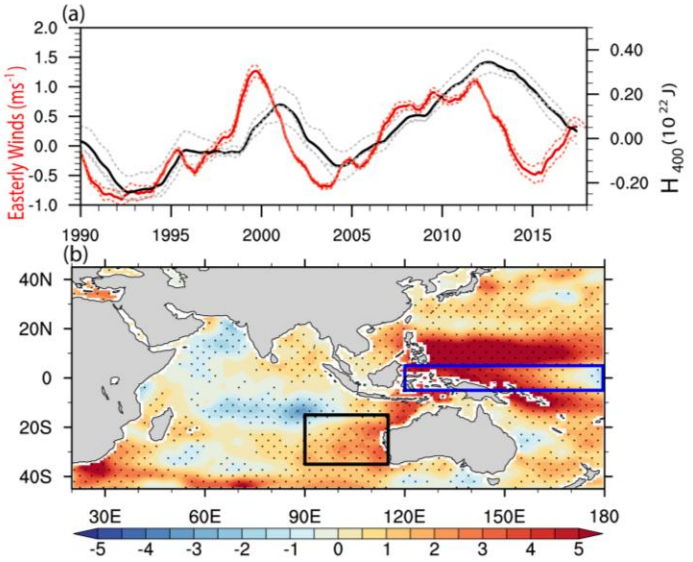

Figure 2. (a) Comparison of western Pacific easterly winds (positive westward) averaged over 120°E -180°E and 5°S-5°N (blue box, Panel b) from NCEP and ERA-Interim (dotted red) with its ensemble mean (solid red) and h_{400} integrated over SEIO (black box, Panel b) from EN4, IAP and WOA (dotted black) and their ensemble mean (solid black). Both the time series are smoothed with 36-months running mean filter. (b) Autoregression between the normalized ensemble mean of easterly winds (positive westward) averaged over 120°E -180°E and 5°S-5°N and h_{400} of the Indo-Pacific basin. Stappling represents region where the regression coefficient is 95% significant based on two-tailed Student's t-test.

warming pattern reasonably well across the decades except for the shallower eastern STIO warming during 1990-1999 compared to observations and also does not show the warming in the Aghulas current region close the African coast in the west.

In order to understand the spatial evolution of the upper ocean heat content trend, we have diagnosed the trends of subsurface temperature across the basin in the STIO for 1990-2018. Figure 1c (and Figure S2) shows the trend in the vertical section of potential temperature across the zonal extent of STIO averaged over 15^{o}S-35^{o}S. During the 1990s, the warming is mostly limited to SEIO close to the west coast of Australia at a rapid rate of ~0.4^{o}C/decade. Noticeably, here the warming trend extends to a deeper depth of ~ 500 m and the maximum warming is seen at ~200-300 m of the subsurface. During the same period, most of the SWIO exhibits a cooling trend of a similar magnitude. On the contrary, the trend calculated for 2000-2018 shows a marked difference from the 1990s. The warming rate in the SEIO weakens considerably, but the warming trend extends further west close to the African coast with maximum warming occurring at the centre of SWIO at a depth of around 100-200 m (Figure 1c; middle panel). While the warming extends down to 400 m in the central and the eastern parts, it shoals towards the west and is limited to about 200 m depth off the eastern edge of the Agulhas current system. The pattern of the warming trends across the STIO during the 1990s and the trends during the last three decades indicate that the warming was initially limited to the coast of Australia, but in the recent decades, this warming has extended into the western part of the basin.

SEIO

Earlier studies have suggested that warming in SEIO is mainly linked to the decadal variability of ITF driven by the easterly winds over the equatorial Pacific associated with IPO (Li et al., 2017). A comparison between the zonal winds averaged over western equatorial Pacific (150^{o}E-180^{o}E, 5^{o}S-5^{o}N; assigning a positive sign to easterlies) and the h_{400} averaged over SEIO indicates that they covary at decadal time scale (Figure 2a) with the heat content of the SEIO lagging a few years from the easterly Pacific winds. Further, regression between the normalized easterly winds with h_{400} of the Indo-Pacific basin (Figure 2b) suggests the impact of these winds strongest in the western Pacific where the variability of the upper ocean heat content is strongly

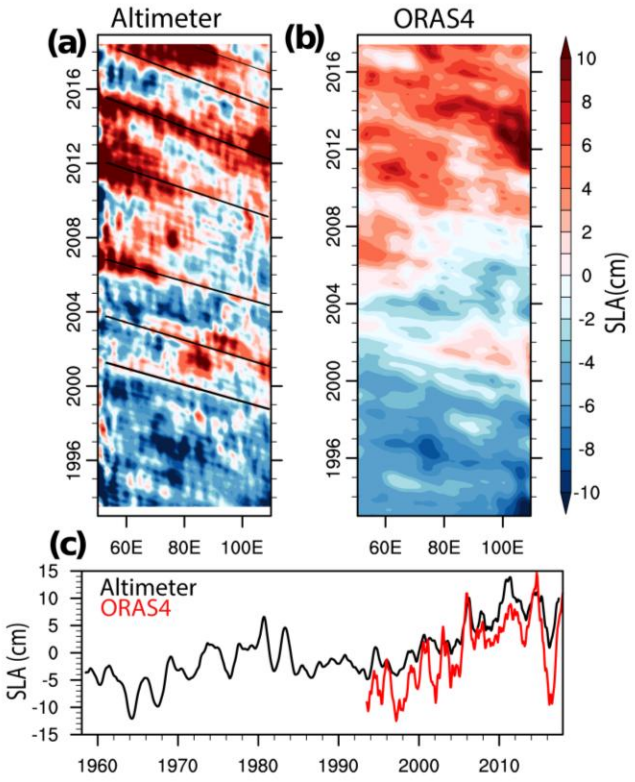

Figure 3. (a) Hövmöller diagram of the altimeter sea level anomaly after removing annual cycle at 25^{o}S. The slanted black lines highlighting the westward propagation of Rossby waves at a speed of 4-6 cm/s. (b) Same as (a) but from ORAS4. (c) Comparison of sea level anomaly after removing annual cycle from altimeter and ORAS4 averaged over STIO.

coupled with the overlying winds. The coupling remains strong along the northwestern and western coasts of Australia via the ITF pathway. The influence of the Pacific winds decreases drastically westward from the Australian coast to remain confined mainly within the SEIO box. In fact, the regression coefficient turns negative in a major portion of the Indian Ocean. Thus, while the decadal variability of the heat content in the SEIO is influenced primarily by the western equatorial Pacific winds, the decadal variability and the warming trend

of the rest of the basin show much weaker relation to the Pacific winds.

SWIO and Southern Ocean Link

Figure 3 shows the Hövmöller diagram of the observed sea level anomaly at 25°S in the STIO with the seasonal cycle removed. The two periods show a marked contrast in the sea level anomaly; while the early 1990s are dominated by a largely negative sea level anomaly, after 2000, sea level anomaly is predominantly positive. Noticeably, altimeter sea level anomaly averaged over the entire STIO shows a rapid increase at a rate of ~4 mm/yr (~5.1 mm/yr in ORAS4) in the latter part of the record (Figure 3c) which is 25% higher than that compared to the global mean sea level rise of ~3.2 mm/yr. A similar rapid increase is also noted in the h_{400} post 2000 (Figure 1b). Further, the phase lines of the sea level anomaly indicate a westward group speed of ~4-6 cm/s which agrees well with the theoretical propagation speed of the lower order vertical modes of the Rossby waves at those latitudes (which is ~5 cm/s at 25°S for the first mode and is given by $\beta c_n^2/f^2$; where $c_n = 264$ cm/s, f is Coriolis parameter and $\beta = \partial f/\partial y$). This suggests that the enhanced sea level in the STIO over the recent decade is driven by these downwelling Rossby waves. The analysis of the longer sea level anomaly record from ORAS4 suggests that the enhanced downwelling Rossby wave propagation is in fact a multi-decadal feature (Figure S3) and existed during the 1970-1985 period as well. However, it is noteworthy that the recent enhancement of sea level propagation is much stronger than the previous period. Figure 4 shows the lag correlation of the sea level anomaly from the altimeter and ORAS4 averaged over a small box (72°E-78°E and 20°S-30°S) in the interior basin of SWIO. The lag correlation for the altimeter derived sea level anomaly is performed for up to 2 years only due to the shorter duration of the data. However, for ORAS4, the lag correlation is computed for up to 5 years. The variability of the sea level anomaly in the SWIO is clearly traced back to the south of Australian coast. This northward tilt of

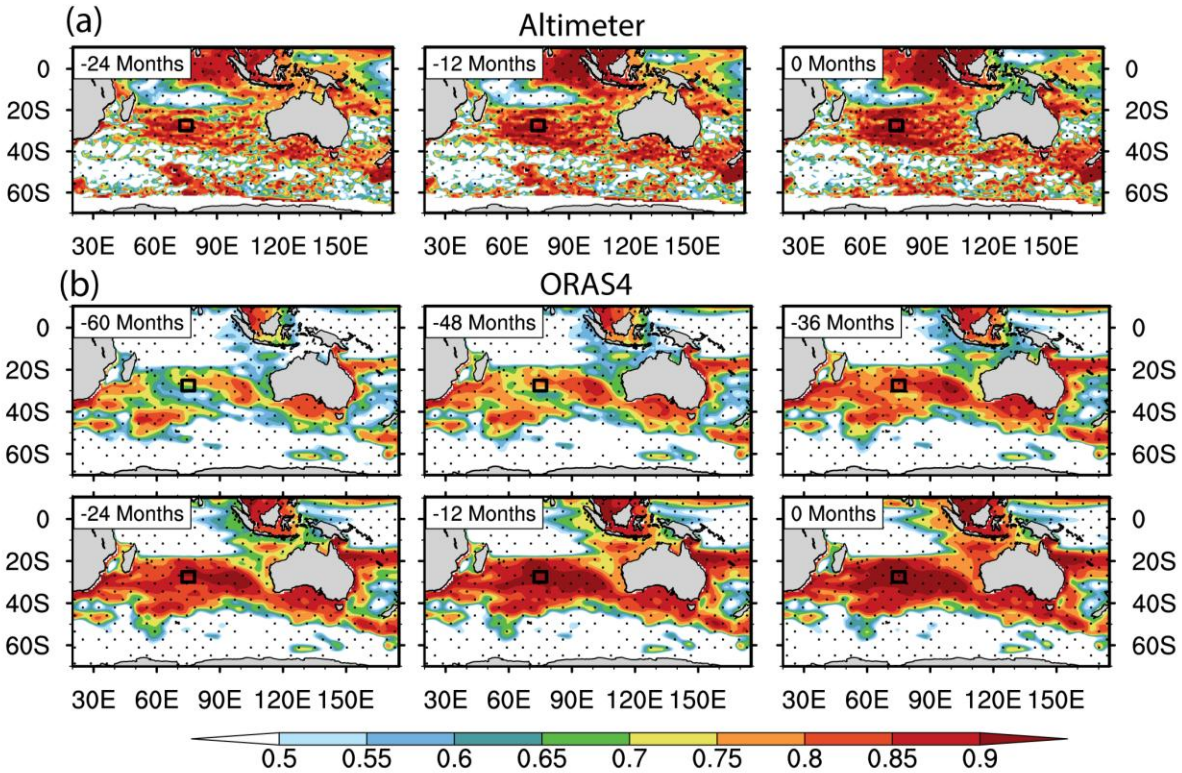

Figure 4. Correlation of the sea level anomaly averaged over 72°E -78°E and 20°S -30°S (black box) to the sea level anomaly of the rest of the basin from (a) altimeter with a lag of 0, 1 and 2 years and from (b) ORAS4 with a lag of 0,1,2,3,4 and 5 years. The dotted region shows 95% significance based on two-tailed t-test. The signals are smoothed using 36-months running mean filter to retain the low frequency signals only.

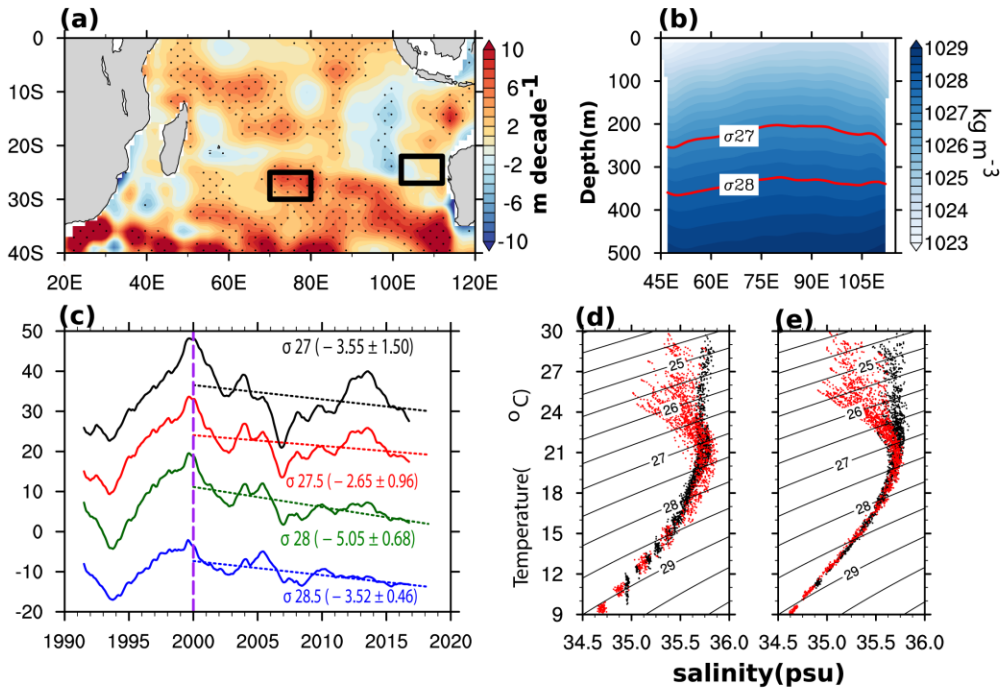

Figure 5. (a) Trend of the σ28 isopycnal layer for the period 2000-2018 from EN4. The near coastal water off the north-west coast of Australia (102°E -112°E/22°S-27°S) and the interior basin within the SWIO (70 °E-80°E/25 °S-30°S) are represented in black boxes to highlight the region with large contrast due to the deepening of the isopycnals in the interior basin over the recent decades. (b) A typical upper water column stratification along the STIO (in this case annual mean for the year 2000). (c) Time series of the difference of the depth of the isopycnals between the coastal waters off the northwest coast of Australia and the interior basin (i.e. east box minus west box of Panel a). This indicates a marked shift in the slope of the isopycnals between SEIO and SWIO after the year 2000. (d) T-S diagram for the top 500 m water column from EN4 for the period 1995-1999 from the western box (black dots) and the eastern box (red dots). (e) Same as (d) but for the period 2014-2018.

the westward propagation is expected from the Rossby wave property where the waves disperse towards the equator as they propagate westward. Interestingly, the correlation analysis did not show a strong connection between the sea level variability of the SWIO to that of the ITF and the western boundary of Australia at decadal frequency. Therefore it suggests that the downwelling Rossby waves in the SWIO are generated south of Australia and not from the Leeuwin Current off the west coast of Australia.

The impact of downwelling Rossby wave is also reflected in the deepening of the observed isopycnal layers in the interior of the STIO (Figure 5a and S4) which leads to an anomalous slope in the pycnoclines in the subsurface layers. A close look at each of the decades (Figure S4) shows a very contrasting balance between SEIO and SWIO. During the 1990s, as the SEIO receives a large amount of extra heat from ITF leading to deepening of thermocline close to the coast of Australia at a rate of ~20 m/decade. Whereas, the thermocline in the SWIO shoaled leading to a steep upward slope of the thermocline from east to west (Figure 5c). In contrast, after 2000, as the thermocline in the centre of STIO started to deepen at a rate of 10-15 m/decade under the influence of the downwelling Rossby waves, isopycnals tilted downward to the west. As a result, warm water from the coast of Australia started to spread westwards into the interior. This feature is more conspicuous in the subsurface water column between σ26.5 to σ28.5 layers where the difference of isopycnal depths between the two regions exhibits an increase at a rate of 3-5 m/decade (Figure 5c). This reversal of pycnocline slope after the year 2000 results in an anomalous westward expansion of warmer water from SEIO to the interior of SWIO. An estimate of volume transport anomaly based on ORAS4 for the subsurface layer indicates that east of 70°E there is a marked change before and after 2000 (Figure S5). While in the 1990s the transport east of 70°E is in general eastward at the rate of ~1 Sv, after 2000, it flipped to predominantly westward at ~-1 Sv creating a change of ~2 Sv across

the decade. This resulted in the distribution of warm subsurface water from the east to SWIO and thereby, helping to warm the interior basin in the recent decade. This can also be seen in the water mass properties of the basin (Figure 5d,e). In the 1990s, water in the SEIO is fresher and warmer compared to the SWIO in the in top 500 m of the water column (above σ29), except in the subsurface layers between σ26.5 to σ28 where the high salinity subsurface core is much saltier in the east than the west. However, after 2000, as anomalous westward flow intensified, the water mass properties across SEIO and SWIO become indistinct below the σ26.5 layer or bellow ~200 m of the water column. Moreover, at the same time properties of the upper water column become more distinct with much fresher water in the east compared to that in the west. This is consistent with the fact that the anomalous westward flow is primarily limited to subsurface layers below the 200m including the thermocline and thereby smearing out the water properties across the STIO at this depth range.

Southern Annular Mode

It is now clear that the Rossby waves generated to the south of Australia drive the transport of extra heat from the SEIO to SWIO and thereby increasing the heat content of the upper water column of the SWIO. The mechanisms that drive the downwelling Rossby waves south of Australia at decadal/multi-decadal periods are diagnosed here.

Over the last few decades, owing to the Southern Ocean warming driven largely by anthropogenic forcing (Cai, 2006), the subpolar low at 65°S deepened rapidly to fall below 980 mbar and thereby helped in a rapid increase of pressure gradient between subtropical high and the subpolar low

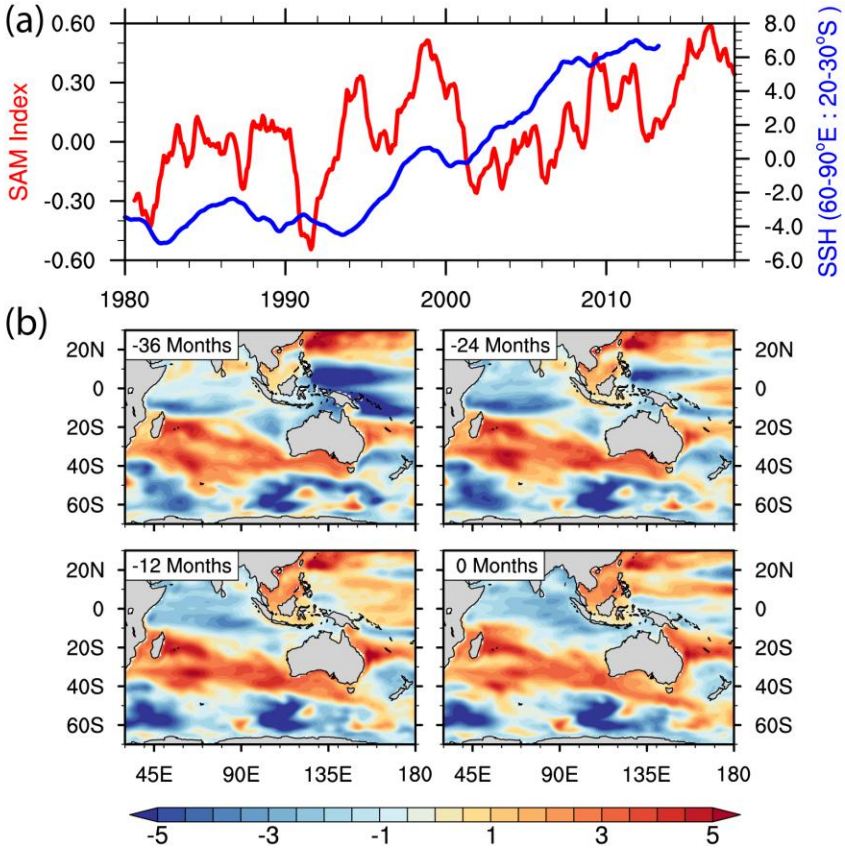

Figure 6. (a) Comparison of SAM and SSH averaged over the interior basin of SWIO. (b) Lag regression of SAM to the SSH anomaly of the entire basin. The top left numbers indicate the number of months lagged applied in the SSH signal from that of the SAM. It is clear that as the lag increases, variability of the SWIO (and to some extent NIO) regression with SAM increases.

(Figure S6a). This resulted in a transition to the positive phase of the Southern Annular Mode (SAM) with stronger westerlies in the 40^{o}S-60^{o}S latitude belt which has strengthened at a rate of 0.32±0.017 m/decade since 1950 (Figure S6b). Additionally, the stronger westerlies, in the presence of the Australian continent to the north, caused a strong shear in the wind field and thus produced a large positive windstress curl around 45^{o}S latitude (Figure S6c). The positive phase of SAM is associated with the poleward shift of the subtropical westerlies which exhibited rapid increase from 1990 onwards with a dip between 1997-2002 and then a persistent positive phase post 2002 (Figure 6a). The SSH anomaly averaged over SWIO shows a remarkable similarity to SAM with a lag of approximately 3 years. This strongly suggests that SAM is playing a key role in modulating the SSH and hence the heat content of the SWIO at decadal frequency. In order to understand this relation further, SAM index is regressed against the SLA of the entire basin (Figure 6b). It clearly shows a strong relationship between SAM and the SLA variability along the latitude band originating from south of Australia to the western boundary of the SWIO caused by positive windstress curl-driven Ekman pumping south of Australia. The windstress curl drives downwelling Rossby waves into the interior of the STIO as shown earlier in the correlation of SLA (Figure 4). Since the curl has grown stronger rapidly after 1990 and in particular after 2005 (Figure S6), the downwelling Rossby waves also intensified in the recent decade across STIO (Figure 3).

Interestingly, as the lag increases, the regression coefficient also increases in the SWIO region and to some extent in the NIO (Figure 6b). It suggests that the decadal variability and the enhancement of the downwelling Rossby waves in the STIO are indeed linked to the variability of SAM and as the lag increases the influence of SAM starts to appear in the NIO as well. In other words, as the positive phase of SAM is strengthening due to anthropogenic forcing, it is generating downwelling Rossby waves south of Australia which are distributing the extra heat from the SEIO to the rest of the Indian Ocean basin.

Conclusions

The upper water column of STIO shows a rapid warming in the last few decades and has become a warming hotspot of the entire Indian Ocean basin. Observations and ocean reanalysis products suggest that warming in STIO is not uniform. While h_{400} from the SEIO shows a prominent decadal variability superposed over a positive trend of $1.75\pm0.19\times10^{21}$ J/decade, the SWIO has warmed monotonically at a relatively rapid pace of $3.71\pm0.17\times10^{21}$ J/decade. No decadal variability is apparent since the year 2000. Moreover, we show that the mechanisms driving the warming of SEIO and SWIO are not the same. As noted earlier, we also find that the secular warming in the SEIO is primarily driven by the decadal variability of the easterly equatorial winds over the western Pacific. The regression analysis suggests that strengthening of easterly winds in the western Pacific advects warm water into the SEIO along the northwestern coast of Australia and thereby increases the heat content of the upper ocean there. Interestingly, this warming was maximum in the late 1990s and confined close to the coast. At the same time, SAM transitioned into a positive phase and has continued to grow in strength through the early 21st century due to the Southern Ocean warming. That has led to enhanced Southern Hemisphere westerlies which in turn has produced a strong positive windstress curl south of Australia. This curl has driven downwelling Rossby waves which propagate into the interior of the STIO. These Rossby waves play a key role in transporting heat from SEIO to SWIO and into the NIO through the cross-equatorial circulation. A schematic of the processes responsible for the distribution of heat in the STIO and subsequently into the entire IO is depicted in Figure 7.

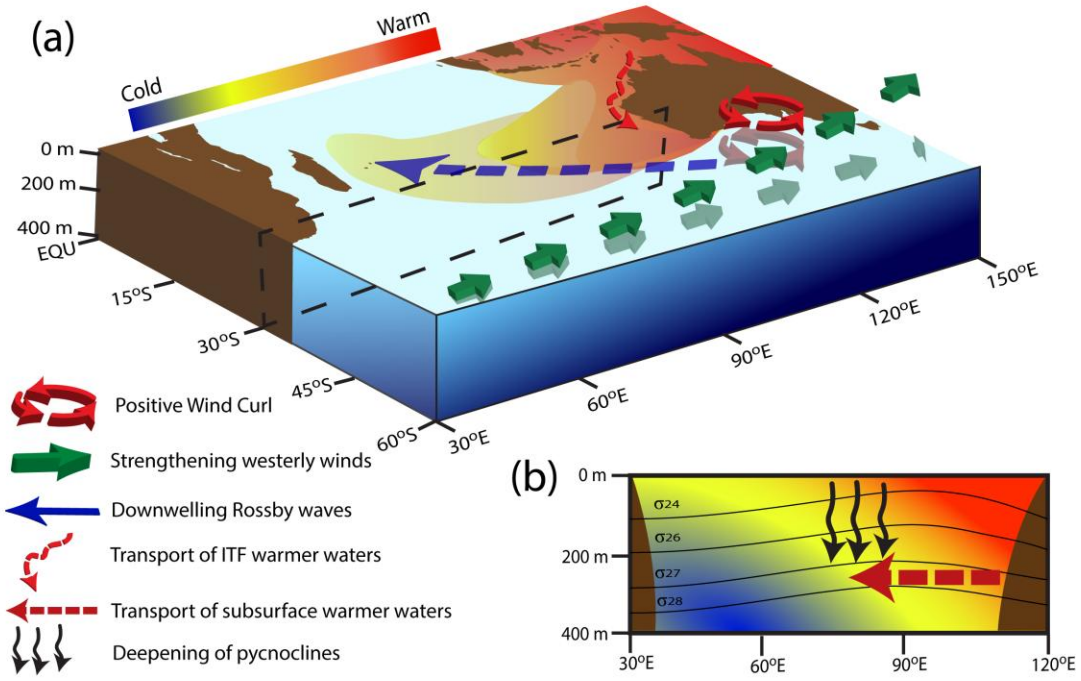

Figure 7. (a) Schematic of the anomalous heat transport in the Indian Ocean. During 1990s the warm water pilled up close to the coast of Australia by the Leeuwin current (the curly arrow). However, as the extratropical westerlies strengthen in the recent decade (green arrows) owing to the Southern Ocean warming driven by the anthropogenic forcing, create a strong positive windstress curl south of Australia (red circular arrows). The positive curl ultimately radiates downwelling Rossby waves into the interior basin (blue arrow). (b) In response to these downwelling Rossby wave radiation, the isopycnals deepen in the interior basin (black downward curly arrows), resulted in downsloping of thermocline from east to west and thereby generating subsurface anomalous westward flow (dark red westward arrow) which helps in redistributing warm water from SEIO to the SWIO and finally to the rest of the north Indian Ocean.

Here, we have unravelled a dynamical link between the Southern Ocean warming and its impact on the Indian Ocean warming. As the Southern Ocean is warming rapidly due to the effect of anthropogenic forcing and thereby westerlies will continue to enhance rapidly (Marshall, 2003; Loveday et al., 2015; Lim et al., 2016), the intensity of the downwelling Rossby waves will likely increase in the future as well. Some studies have now shown that the Indian Ocean warming is impacting the Pacific Ocean's response to anthropogenic forcing as well the Atlantic Meridional Overturning Circulation (Luo et al., 2012; Hu and Fedorov, 2019). The complex pathways of variability and trends from the tropical Pacific and the Southern Ocean into the Indian Ocean and from the Indian Ocean back to the Pacific and the Atlantic indicate that the Indian Ocean may be playing an outsized role in climate variability and change. Future studies need to fully deconvolve these feedbacks including the impacts of the Indian Ocean warming on the monsoon and the Indian Ocean cyclones. Considering the very high vulnerability of the Indian Ocean rim countries, the importance of these findings can hardly be overemphasized.

Methods

Here we discuss the observations, model reanalysis product and the statistical techniques used in this study.

Observations

To estimate the variability and trend of the upper water column temperature and heat content we have used three objectively analysed temperature and salinity data products: (a) The ENACT/ENSEMBLES Version 4 (EN4) provided by Met Office (Good et al., 2013), (b) World Ocean Atlas 2009 (WOA) provided by National Oceanic and Atmospheric Administration (NOAA; Levitus et al., 2012) and (c) the Institute of

Atmospheric Physics (IAP) ocean temperature analysis (Cheng et al., 2016, 2017). While the data from EN4 is used as the primary source of understanding, the other two gridded products are used to support the conclusions wherever possible. All these datasets are available at 1^o X 1^o grid globally and are analysed for 1979-2018. While EN4 and IAP data sets are available at a monthly frequency, the WOA data set is available only as a quarterly time series. Also, note that salinity data from WOA is available only from 2005 and for IAP it is limited to the top 700 m of the water column. For atmospheric flux calculations, data from NCEP-NCAR (kalnay et al., 1996) and ERA-Interim (Dee et al., 2011) are used. The gridded 4^{th} Level Sea level anomaly data are obtained from AVISO (https://www.aviso.altimetry.fr/) for the period 1993-2019.

Ocean Reanalysis

In addition to observations, to analyse a longer period, we have also used an ocean reanalysis product, ORAS4 (Balmaseda et al., 2013). ORAS4 is based on NEMO (Nucleus for European Modelling of the Ocean) (Madec, 2015) ocean model and uses a variational data assimilation system (NEMOVAR; Mogensen et al., 2012). NEMO has a resolution of 0.3^o in the tropics and 1^o in the extratropical regions. The model assimilates temperature/salinity profiles and along track altimeter data. Model is forced by the daily surface fluxes from European Center for Medium Range Weather Forecasts (ECMWF) reanalysis system. ORAS4 is available at $1^o \times 1^o$ horizontal resolution and extends from 1948 to 2017. It is downloaded from Asia-Pacific Data-Research Centre (APDRC) of the IPRC (http://apdrc.soest.hawaii.edu/data/data.php). ORAS4 is shown to be one of the best ocean reanalysis product and is validated extensively over the Indian Ocean (Jayasankar et al., 2019a).

Ocean Heat Content and Anomaly

We have computed the upper ocean heat content for the top 400 m water column (h_{400}) using the equation

$$h_{400}(x,y,t) = C_p \int_{-400}^{0} \rho(x,y,z,t)\theta(x,y,z,t)\mathrm{d}z$$

where, C_p is the specific heat capacity of seawater 3850 J kg^{-1} C^{-1}, ρ is the potential density of seawater computed from potential temperature (θ, ^{o}C) and practical salinity (psu). The anomalies are computed using a mean for the period 1980-2018. The depth integrated h_{400} anomalies are further integrated over spatial regions to yield timeseries (in Figure 1b). Note all the variables are smoothed by a 3 year running mean filter unless otherwise stated.

Trends and Statistical significance

Linear trends are calculated based on linear regression analysis. For statistical significance, we have used the criterion of correlation significance of the regressed line to the actual time series. The regressed line is considered significant if the critical value of the correlation coefficient, calculated using the formula $= \frac{r\sqrt{n-2}}{\sqrt{1-r^2}}$, is greater than or equal to the corresponding value in the two-tailed t-table for the degrees of freedom and the desired confidence interval. Where "r" represents the correlation coefficient and $n-2$ represents the degrees of freedom.

Code availability

Data processing codes and the processed data are available from the corresponding author upon request.

Acknowledgments

We gratefully acknowledge the funding support given by Indian National Centre for Ocean Information Services (INCOIS), Ministry of Earth Sciences to carry out the research. S.C.K. is funded by Centre for Science and Industrial Research fellowship towards his doctoral degree. RM gratefully acknowledges the Visiting Faculty position at the Indian Institute of Technology, Bombay. This is INCOIS contribution number XXXX.

Author contributions

A.C. designed the study. A.C. and S.C.K. analysed the data and made the plots. All authors contributed ideas in developing the research, discussed the results and jointly wrote the paper.

Competing interests

The authors declare no competing interests.

References

Balmaseda M. A., Mogensen K., Weaver A. T. Evaluation of the ECMWF ocean reanalysis system ORAS4. Q J R Meteorol Soc 139:1132–1161. doi:10.1002/qj.2063 (2013).

Birol, F., and Morrow R. Source of the baroclinic waves in the southeast Indian Ocean, J. Geophys. Res., **106**, 9145– 9160 (2001).

Cai W., Meyers G. and Shi G. Transmission of ENSO signal to the Indian Ocean. Geophys. Res. Lett. **32** (L05616). https://doi.org/10.1029/2004GL021736 (2005).

Cai W. Antarctic ozone depletion causes an intensification of the Southern Ocean super-gyre circulation, Geophys. Res. Lett. **33**, L03712, doi:10.1029/2005GL024911 (2006).

Cheng, L., Abraham, J., Goni, G., Boyer, T., et al. XBT Science: Assessment of instrumental biases and errors. Bulletin of the American Meteorological Society, **97**, 924–933 (2016).

Cheng, L., Trenberth, K., Fasullo, J., Boyer, T., Abraham, J., and Zhu, J. Improved estimates of ocean heat content from 1960 to 2015. Science Advances, **3**, e1601545 (2017).

Dee, D., Uppala, S., Simmons, A., Berrisford, P., Poli, P., Kobayashi, S. et al. The ERA-Interim reanalysis: Configuration and performance of the data assimilation system. Quarterly Journal of the Royal Meteorological Society, 137(656), 553–597 (2011).

Dong L. and McPhaden M. J. Interhemispheric SST gradient trends in the Indian Ocean prior to and during the recent global warming hiatus. J. Climate. **30**. 1971–1983, https://doi.org/10.1175/JCLI-D-16-0313.1 (2017).

England, M. H., McGregor, S., Spence, P., Meehl, G. A., Timmermann, A., Cai, W., et al. Recent intensification of wind-driven circulation in the Pacific and the ongoing warming hiatus. Nature Climate Change, 4(3), 222–227. https://doi.org/10.1038/nclimate2106 (2014).

Feng M., McPhaden M. J., Xie S.-P. and Hafner J. La Niña forces unprecedented Leeuwin Current warming in 2011. Sci. Rep. **3**, https://doi.org/10.1038/srep01277 (2013).

Feng M., Hendon H. H., Xie S.-P., Marshall A. G., Schiller A., Kosaka Y., Caputi N. and Pearce A. Decadal increase in Ningaloo Niño since the late 1990s. Geophys. Res. Lett. **42**, 104–112, https://doi.org/10.1002/2014gl062509 (2015).

Han, W., Vialard, J., McPhaden, M. J., Lee, T., Masumoto, Y., Feng, M., and de Ruijter, W. P. M. Indian Ocean decadal variability: A review. Bulletin of the American Meteorological Society, 95, 1679–1703 (2014).

Han W., Webster P. J., Stammer D., Hu A., Hamlington B., Kenigson J., Palanisamy H. and Thompson P. Spatial patterns of sea level variability associated with natural internal climate modes. Surv. Geophys. **38**, 217–250, https://doi.org/10.1007/s10712-016-9386-y (2017).

Hirst, A. C., and Godfrey, J. The role of Indonesian Throughflow in a global ocean GCM. Journal of Physical Oceanography, **23**(6), 1057–1086.https://doi.org/10.1175/15200485(1993)023<1057:TROITI>2.0.CO;2 (1993).

Hu, S. and Fedorov, A.V. Indian Ocean warming can strengthen the Atlantic meridional overturning circulation. Nat. Clim. Chang. **9,** 747–751. https://doi.org/10.1038/s41558-019-0566-x (2019).

Jayasankar T., Eldho T.I., Ghosh S. and Murtugudde R. Assessment of the interannual variability of local atmospheric and ITF contribution to the subsurface heat content of southern tropical Indian Ocean in GECCO2 and ORAS4 using ROMS. Global and Planetary Change, **181**, https://doi.org/10.1016/j.gloplacha.2019.05.014 (2019a).

Jayasankar T., Murtugudde R., and Eldho T. I. The Indian Ocean Deep Meridional Overturning Circulation in Three Ocean Reanalysis Products. Geophys. Res. Lett. **46**, ttps://doi.org/10.1029/

2019GL084244 (2019b).

Kalnay, E., Kanamitsu, M., Kistler, R., Collins, W., Deaven, D., Gandin, L. et al. The NCEP/NCAR 40-year reanalysis project. Bulletin of the American Meteorological Society, 77(3), 437–471 (1996).

Katsman C. A. and Oldenborgh Van G. J. Tracing the upper ocean's "missing heat". Geophys. Res. Lett. 38 (L14610), doi:10.1029/2011GL048417 (2011).

Lee S.-K. et al. Pacific origin of the abrupt increase in Indian Ocean heat content. Nature Geoscience, **8**, 445-449 (2015).

Levitus S., Antonov J. I., Boyer T. P., et al. World ocean heat content and thermosteric sea level change (0–2000 m), 1955–2010: WORLD OCEAN HEAT CONTENT. Geophys Res Lett 39: doi:

10.1029/2012GL051106 (2012).

Li, Y., Han, W. and Zhang, L. Enhanced decadal warming of the southeast Indian Ocean during the recent global surface warming slowdown. Geophys. Res. Lett., **44**, 9876–9884. https://doi.org/10.1002/2017GL075050 (2017).

Li Y., Han W., Hu A., Meehl G. and Wang F. Multidecadal changes of the upper Indian Ocean heat content during 1965–2016. J. Clim. **31**, 7863–7884, https://doi.org/10.1175/JCLI-D-18-0116.1 (2018).

Li Y., Han W., Zhang, L. and Wang F. Decadal SST Variability in the Southeast Indian Ocean and Its Impact on Regional Climate. J. Clim. https://doi.org/10.1175/JCLI-D-19-0180.1 (2019).

Liu W., Xie, S.-P. and Lu, J. Tracking ocean heat uptake during the surface warming hiatus. Nature Comm. **7** (10926), https://doi.org/10.1038/ncomms10926 (2016).

Loveday B. R., Penven P., and Reason C. J. C. Southern Annular Mode and westerly-wind-driven

changes in Indian-Atlantic exchange mechanisms, Geophys. Res. Lett. **42**, 4912–4921, doi:10.1002/2015GL064256 (2015).

Lim E.-P., Hendon H. H., Arblaster J. M., Delage F., Nguyen H., Min S.-K., and Wheele M. C. The impact of the Southern Annular Mode on future changes in Southern Hemisphere

rainfall, Geophys. Res. Lett., 43, 7160–7167, doi:10.1002/2016GL069453 (2016).

Luo, J. J., Sasaki, W. & Masumoto, Y. Indian Ocean warming modulates Pacific climate change. Proc. Natl Acad. Sci. USA **109**, 18701–18706 (2012).

Madec G. NEMO ocean engine. Note du Pole de modélisation de l' Institut Pierre-Simon Laplace, Paris, France, 27, 401 pp, hdl:10013/epic.46840.d001 (2015).

Marshall G. J. Trends in the Southern Annular Mode from observations and reanalyses, J. Clim. **16**, 4134–4143 (2003).

Meehl, G., Arblaster, J., Fasullo, J. *et al.* Model-based evidence of deep-ocean heat uptake during surface-temperature hiatus periods. *Nature Clim Change* **1,** 360–364, https://doi.org/10.1038/nclimate1229 (2011).

Meehl, G. A., and Teng H. CMIP5 multi-model hindcasts for the mid-1970s shift and early 2000s hiatus and predictions for 2016–2035. Geophys. Res. Lett., **41**, 1711–1716, doi:10.1002/ 2014GL059256 (2014).

Mogensen K., Balmaseda A. M., Weaver A. The NEMOVAR ocean data assimilation system as implemented in the ECMWF ocean analysis for System 4. European Centre for Medium-Range Weather Forecasts (2012).

Nieves V., Willis J. K. and Patzert W. C. Recent hiatus caused by decadal shift in Indo-Pacific heating. Science, **349** (6247), 532-535 (2015).

Potemra, J. T. The potential role of equatorial Pacific winds on southern tropical Indian Ocean Rossby waves, J. Geophys. Res., **106**, 2407–2422 (2001).

Roser M., Ritchie H. and Esteban O.-O. World Population Growth. Our World in Data, https://ourworldindata.org/world-population-growth (2020).

Srinivasu U., Ravichandran M., Han W., Sivareddy S., Rahman1 H., Li Y. and Nayak S. Causes for the reversal of North Indian Ocean decadal sea level trend in recent two decades. Clim. Dyn., 49, 3887-3904, 10.1007/s00382-017-3551-y (2017).

Thompson, P. R., Piecuch C. G., Merrifield M. A., McCreary J. P., and Firing E. Forcing of recent decadal variability in the Equatorial and North Indian Ocean. J. Geophys. Res. (Oceans), 121, 6762–6778, doi:10.1002/2016JC012132 (2016).

Trenberth, K. E., and Fasullo, J. T. An apparent hiatus in global warming? Earth's Future, 1(1), 19–32. https://doi.org/10.1002/2013EF000165 (2013).

Vidya P. J., Ravichandran M., Subeesh M. P., Chatterjee S.. and Nuncio M. Global warming hiatus contributed weakening of the Mascarene High in the Southern Indian Ocean. Sci. Rep. **10** (3255), https://doi.org/10.1038/s41598-020-59964-7 (2020).

Wijffels S. and Meyers G. An intersection of oceanic waveguides: Variability in the Indonesian Throughflow region. J. Phys. Oceanogr. **34**, 1232-1253 (2004).

Zhang Y., Feng, M., Du, Y., Phillips, H. E., Bindoff, N. L., and McPhaden, M. J. Strengthened Indonesian Throughflow Drives Decadal Warming in the Southern Indian Ocean. Geophys. Res. Lett. **45**, 6167–6175. https://doi.org/10.1029/2018GL078265 (2018).

Zinke J, Hoell A, Lough JM et al. Coral record of southeast Indian Ocean marine heatwaves with intensified Western Pacific temperature gradient. Nat Commun 6:1–9. https://doi.org/10.1038/ncomms9562 (2015).